Electronic Supplementary Information for

Self-assembled Transition Metal Chalcogenides@CoAl-LDH 2D/2D Heterostructures with Enhanced Photoactivity for Hydrogen Evolution

Linfen Peng[a], Changqiang Yu[a], Yuheng Ma[a], Guanshun Xie[a], Xiuqiang Xie[a, *], Zhenjun Wu[b, *], Nan Zhang[a, *]

[a]*College of Materials Science and Engineering, Hunan University, Changsha 410082, China*

[b]*College of Chemistry and Chemical Engineering, Hunan University, Changsha 410082, China*

*Corresponding author, E–mail: xiuqiang_xie@hnu.edu.cn; wooawt@hnu.edu.cn; nanzhang@hnu.edu.cn

Contents list

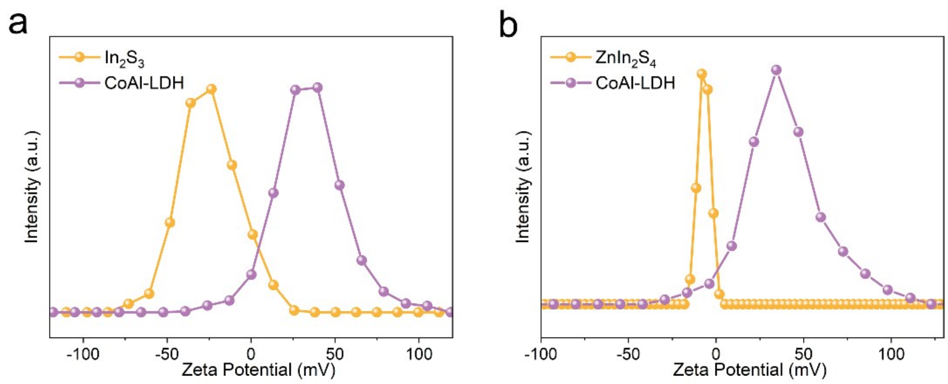

Figure. S1. Zeta Potentials.

Note: The CoAl-LDH nanosheets have a positive zeta potential of +49.3 mV, whereas the In_2S_3 nanosheets have a negative zeta potential of −19.6 mV and the $ZnIn_2S_4$ nanosheets have a negative zeta potential of -8.1 mV.

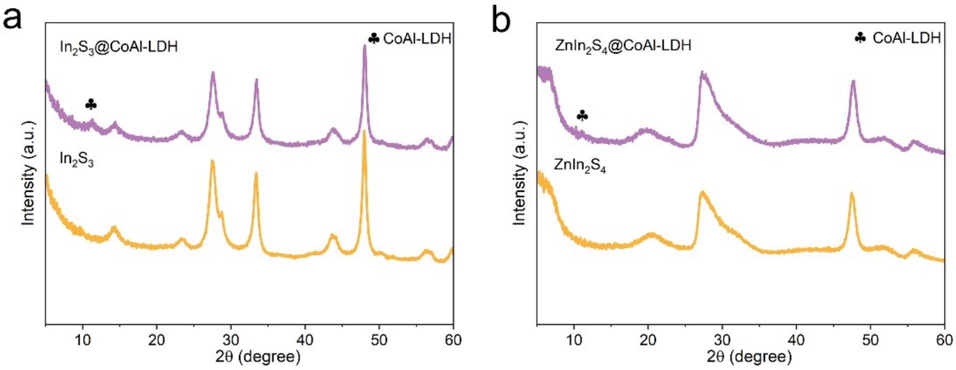

Figure. S2. XRD patterns of the synthesized In_2S_3, In_2S_3@CoAl-LDH, $ZnIn_2S_4$, and $ZnIn_2S_4$@CoAl-LDH.

Note: As shown in Figure. S2a, The XRD patterns of In_2S_3@CoAl-LDH and pristine In_2S_3 could be indexed to the cubic phase of In_2S_3(JCPDS No. 65-0459)[1], the peaks at 2θ = 14.2°, 23.3°, 27.4°, 28.7°, 33.2°, 43.6°, 47.7°, 56.6°, 59.4°of bare In_2S_3 are indexed to the (111), (220), (311), (222), (400), (511), (440), (622) and (444) crystal planes, respectively. Figure. S2b shows the XRD patterns of $ZnIn_2S_4$ and $ZnIn_2S_4$@CoAl-LDH heterostructure, wherein obvious diffraction peaks at 20.5°, 27.6°, 47.6° and 56° correspond to the (006), (102), (112) and (202) crystal planes of hexagonal $ZnIn_2S_4$ (JCPDS No. 01-072-0773)[2], respectively.

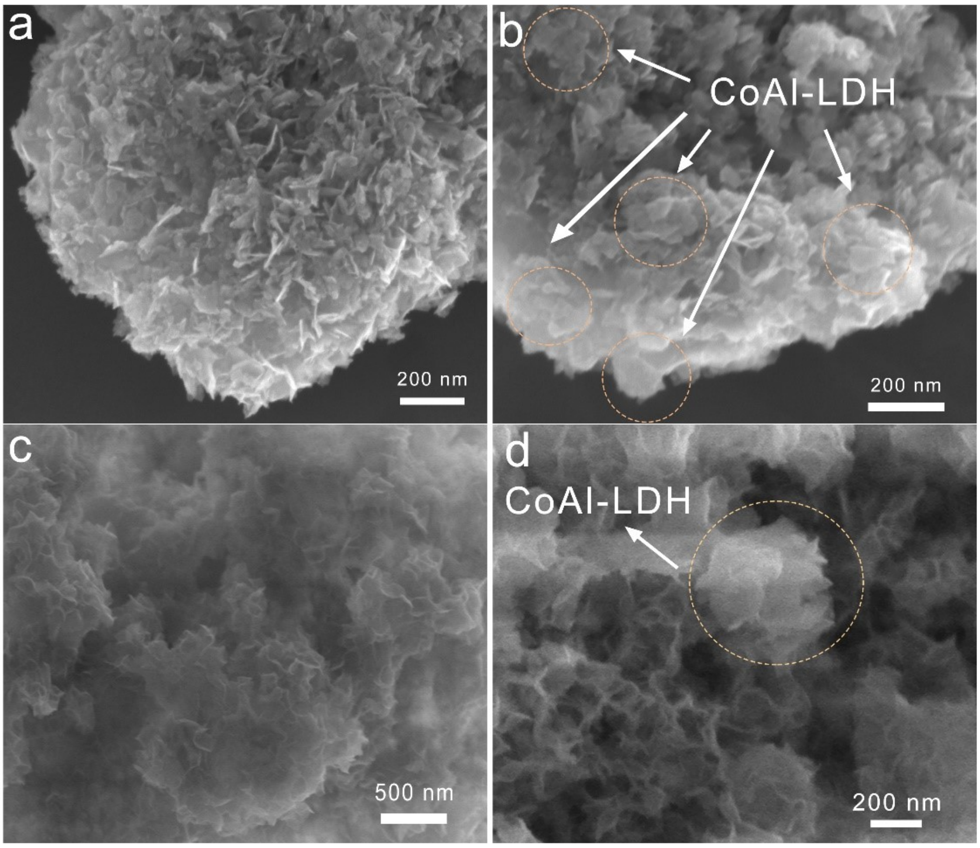

Figure. S3. SEM images of In_2S_3 (a), In_2S_3@CoAl-LDH (b), $ZnIn_2S_4$ (c), and $ZnIn_2S_4$@CoAl-LDH (d).

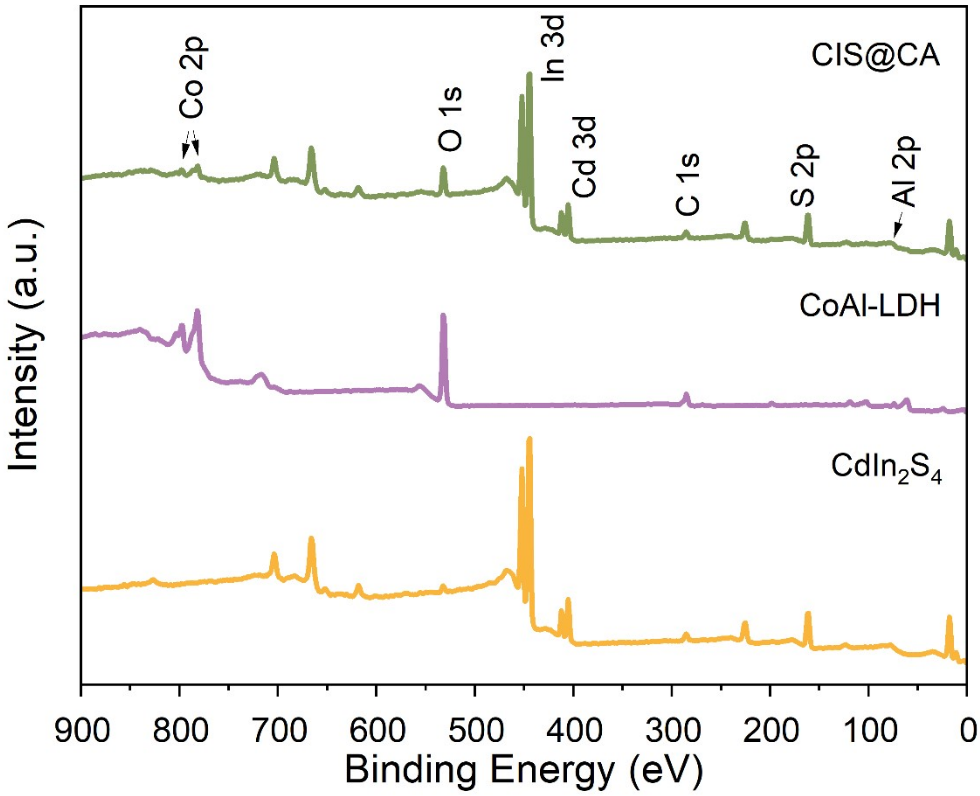

Figure. S4. XPS survey spectra of $CdIn_2S_4$ NSs, CoAl-LDH and CIS@CA composites.

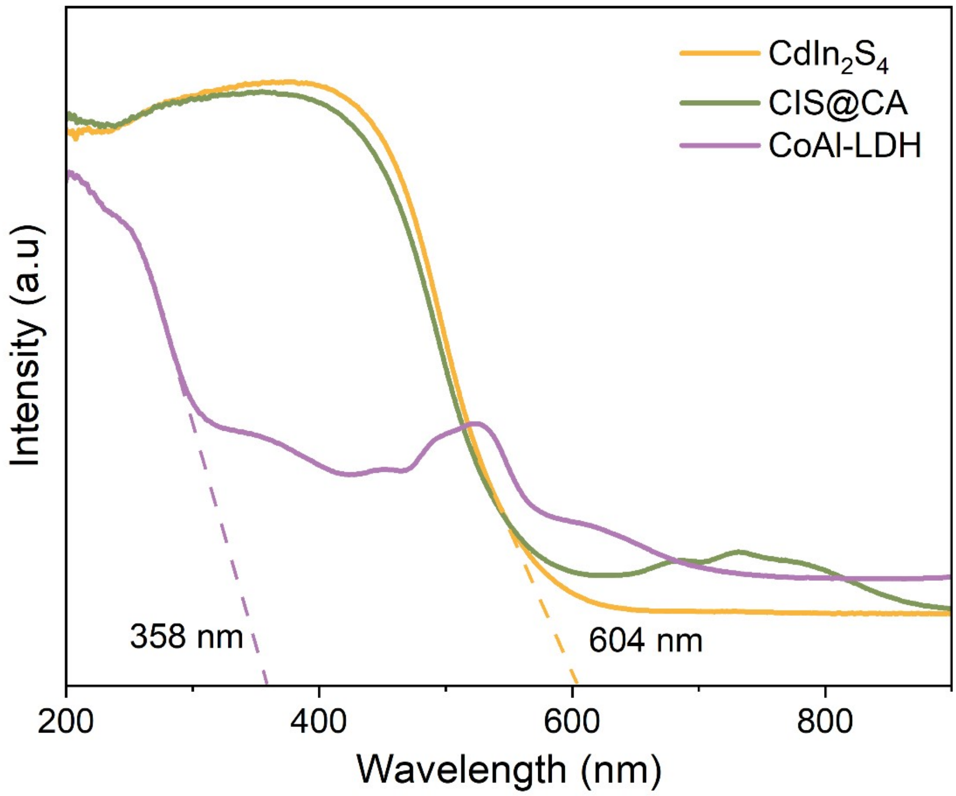

Figure. S5. DRS spectra of bare $CdIn_2S_4$, bare CoAl-LDH, and CIS@CA composites.

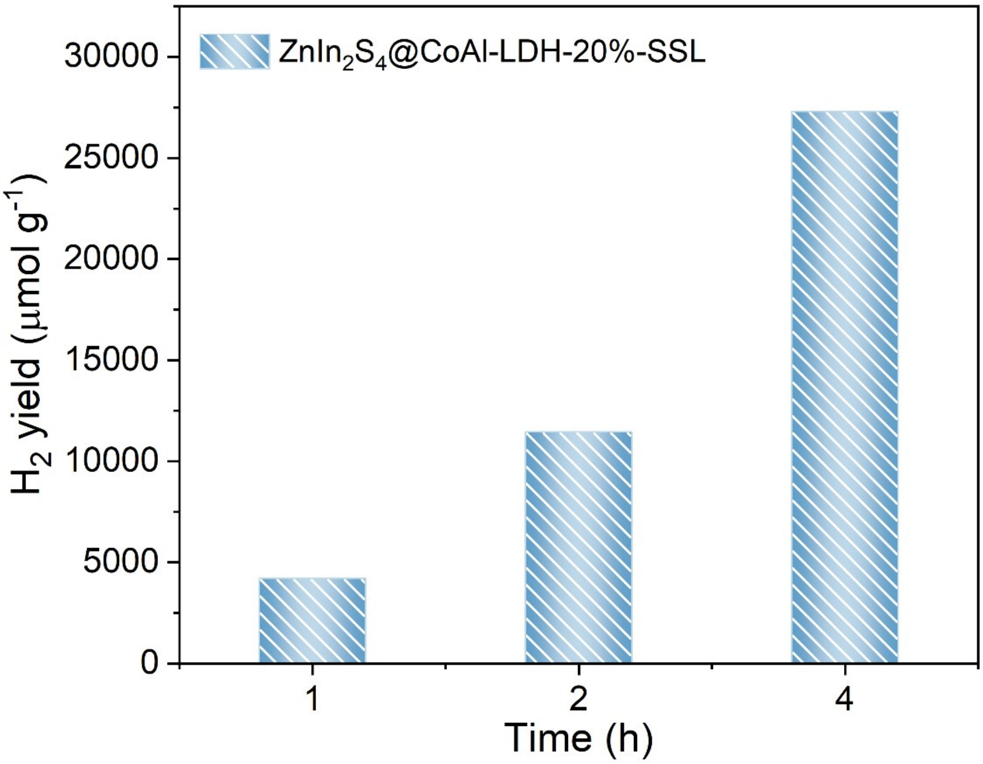

Figure. S6. Photocatalytic activity of $ZnIn_2S_4$@CoAl-LDH-20% composites for H_2 production under SSL irradiation.

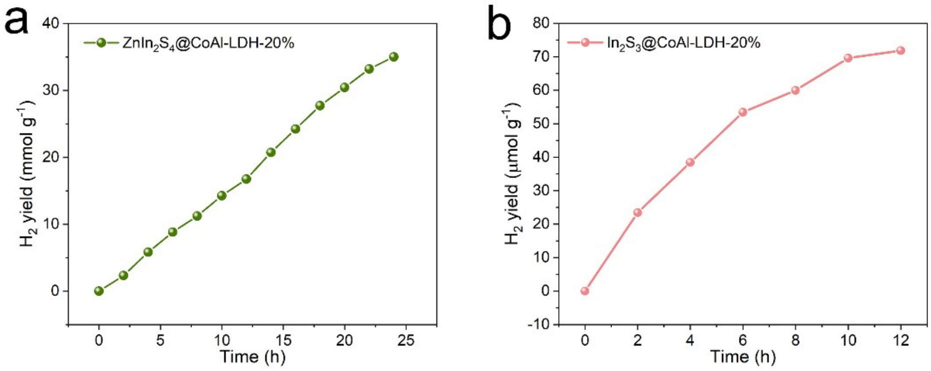

Figure S7. Long-time stability of $ZnIn_2S_4$@CoAl-LDH-20% and In_2S_3@CoAl-LDH-20% for photocatalytic H_2 production.

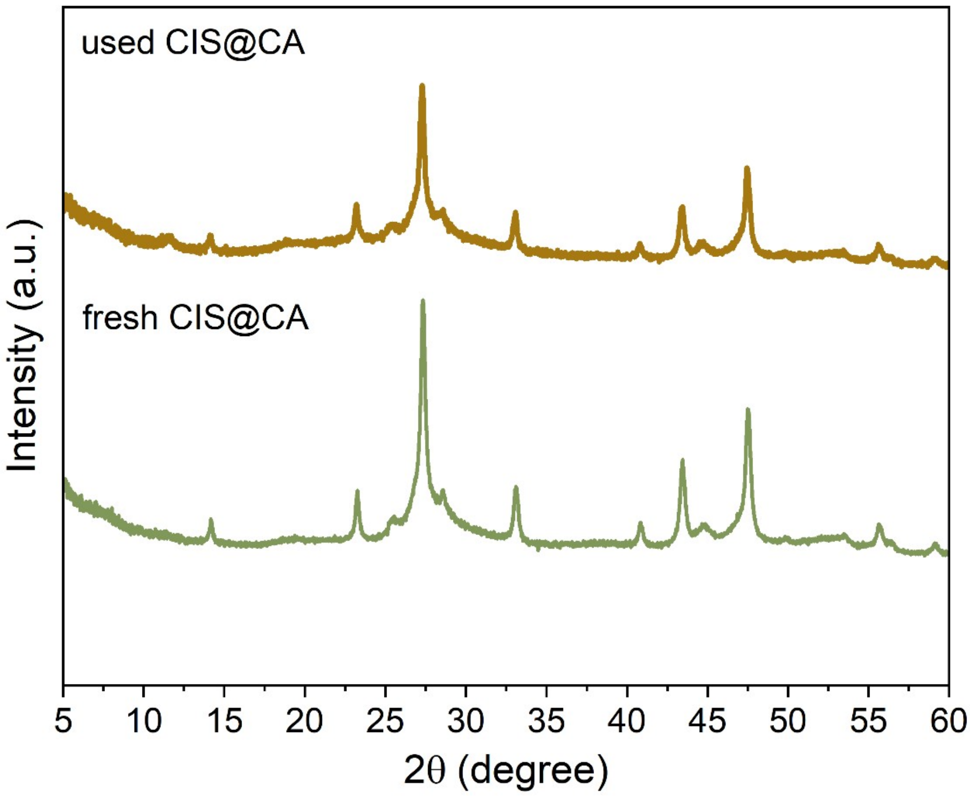

Figure. S8. XRD patterns of fresh and used CIS@CA composites.

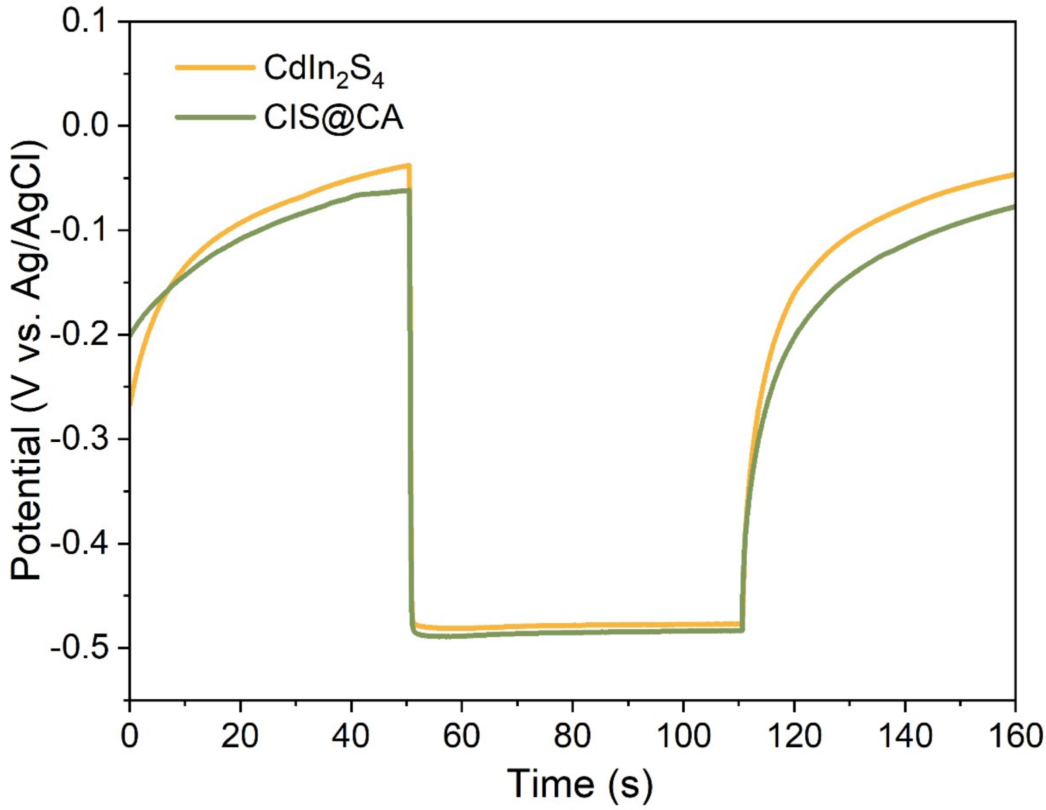

Figure. S9. Decay curves of photovoltage.

Supplementary Note: The photoelectron lifetime (τ_n) is calculated by the following formula[3]:

$$\tau_n = (k_B T/e)(dV_{OC}/dt)^{-1}$$

where k_B, T, e, V_{OC} and t are Boltzmann's constant (1.3806×10^{-23} J/K), charge of one electron (1.602×10^{-19} C), temperature (298.15 K), open circuit photovoltage and time, respectively.

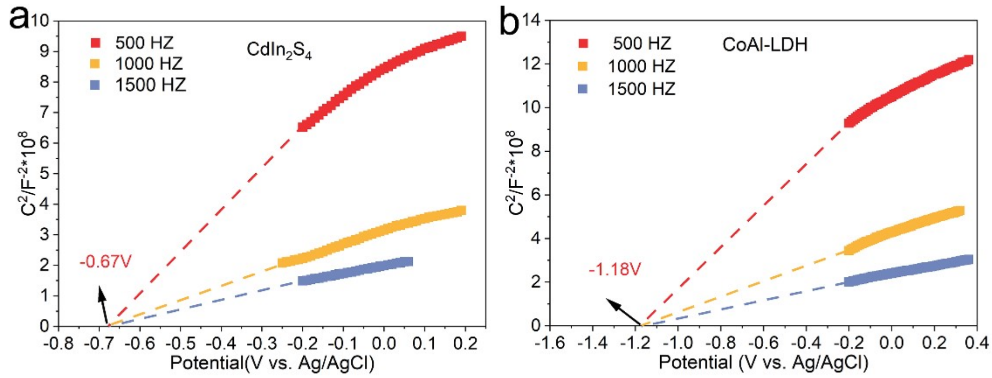

Figure. S10. Mott-Schottky plots for $CdIn_2S_4$ (a) and CoAl-LDH (b).

Supplementary Note:The flat-band potential values (E_{fb}) can be determined by the following Mott−Schottky equation[4]:

$$\frac{1}{C^2} = \frac{2}{\varepsilon\, \varepsilon_0 N_D}\left(E - E_{fb} - \frac{k_B T}{q}\right)$$

where ε and ε_0 are the dielectric constants of free space and the film electrode, and N_D, C, E, T, k_B, and q represent the donor density, space charge capacitance, applied potential, temperature, Boltzmann's constant, and electronic charge, respectively.

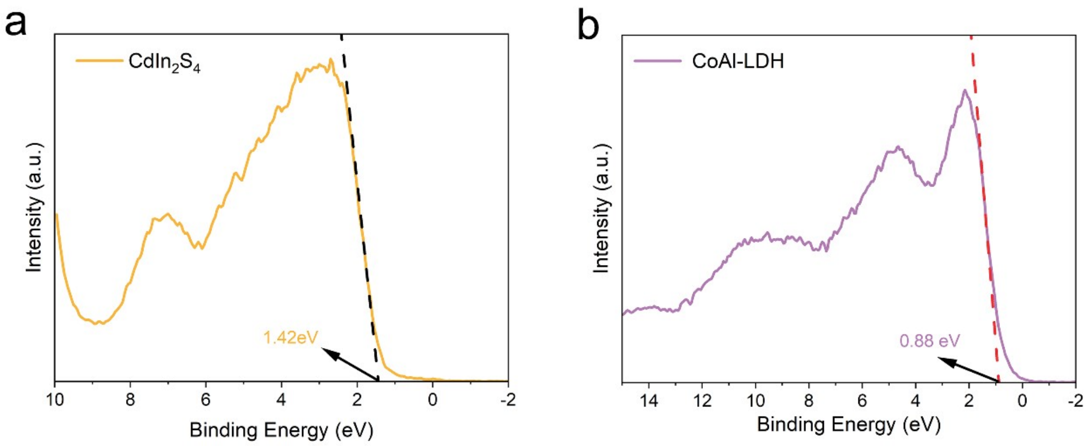

Figure. S11. (a) VB XPS curves of $CdIn_2S_4$ and (b) CoAl-LDH.

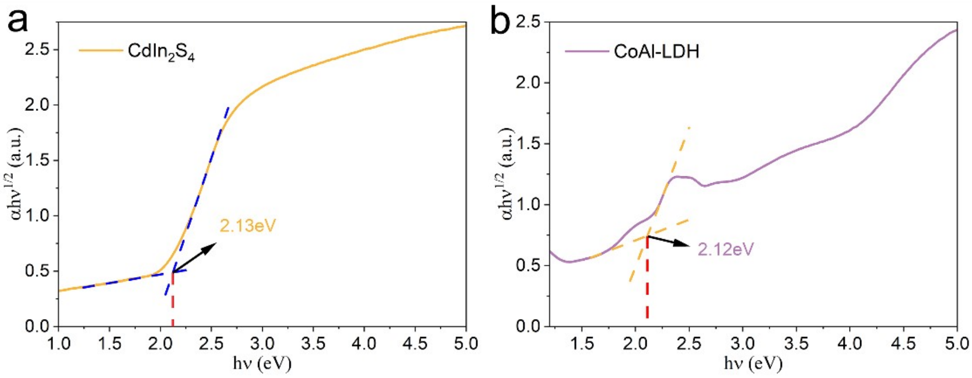

Figure. S12. The estimated band gap energy of $CdIn_2S_4$ (a) and CoAl-LDH (b) based on the Kubelka-Munk function plot transformed from the absorbance.

Supplementary Note: The Kubelka−Munk equation is employed to calculate the band gap energy of the as-obtained solid solutions[4, 5]:

$$(\alpha h\nu)^{1/n} = A(h\nu - E_g)$$

where h, α, ν, A, and E_g represent Planck's constant (6.63×10^{-34} J · s), optical absorption coefficient, photon frequency, a constant, and photonic energy band gap, respectively. In addition, n is 2 for a direct band gap and 1/2 for an indirect band gap.

References

1. Y. Zhu, G. Xie, G. Li, F. Song, C. Yu, Z. Wu, X. Xie and N. Zhang, Facial synthesis of two-dimensional $In_2S_3/Ti_3C_2T_x$ heterostructures with boosted photoactivity for the hydrogenation of nitroaromatic compounds, *Mater. Chem. Front.*, 2021, **5**, 6883-6890.
2. H.-J. Lin, Q.-L. Mo, S. Xu, Z.-Q. Wei, X.-Y. Fu, X. Lin and F.-X. Xiao, Unlocking photoredox selective organic transformation over metal-free 2D transition metal chalcogenides-MXene heterostructures, *J. Catal.*, 2020, **391**, 485-496.
3. J.-Y. Li, Y.-H. Li, F. Zhang, Z.-R. Tang and Y.-J. Xu, Visible-light-driven integrated organic synthesis and hydrogen evolution over 1D/2D CdS-$Ti_3C_2T_x$ MXene composites, *Appl. Catal. B: Environ.*, 2020, **269**, 118783.
4. C. Zeng, H. W. Huang, T. R. Zhang, F. Dong, Y. H. Zhang and Y. M. Hu, Fabrication of Heterogeneous-Phase Solid-Solution Promoting Band Structure and Charge Separation for Enhancing Photocatalytic CO_2 Reduction: A Case of $Zn_xCa_{1-x}In_2S_4$, *ACS Appl. Mater. Interfaces*, 2017, **9**, 27773-27783.
5. C. Zeng, Y. M. Hu, T. R. Zhang, F. Dong, Y. H. Zhang and H. W. Huang, A core-satellite structured Z-scheme catalyst $Cd_{0.5}Zn_{0.5}S/BiVO_4$ for highly efficient and stable photocatalytic water splitting, *J. Mater. Chem. A*, 2018, **6**, 16932-16942.